Digital Multiplierless Realization of Two-Coupled Biological Hindmarsh–Rose Neuron Model

Mohsen Hayati, Moslem Nouri, Derek Abbott, *Fellow, IEEE*, and Saeed Haghiri

***Abstract*—The efficient modeling, simulation, and implementation of biological neural networks are key objectives of the neuromorphic research field, leading to potential applications, such as assisting the search for new solutions to cure brain diseases, improved performance of robots, and the fundamental study of neural network behavior. This brief proposes a modified biological Hindmarsh–Rose (HR) neuron model that is more suited for efficient implementation on digital platforms. Simulation results show that the model can reproduce the desired behaviors of the neuron. The proposed model is investigated, in terms of digital implementation feasibility and cost, targeting a low-cost hardware implementation. Hardware implementation on a field-programmable gate array shows that the modified model mimics the biological behavior of different types of neurons, with higher performance and considerably lower hardware overhead cost compared with the original HR model.**

***Index Terms*—Field-programmable gate array (FPGA), Hindmarsh–Rose (HR) neuron model, spiking neural network (SNN).**

I. Introduction

THE increased fundamental understanding of neural network architectures in the brain is one of the motivations of exploring hardware implementations of neuronal models [1]–[10]. In order to mimic and hence understand aspects of brain behavior, one may consider a system that includes a large number of primary building blocks and the basic signaling unit of the nervous system, neurons, which are connected to each other in an intricate pattern in the brain [11].

For the simulation and implementation of these complex architectures, mathematical modeling of neural dynamics and spiking-neural-network mechanisms have been used in the analysis of neuron behavior [12]. In this case, the behavior of a single neuron can be explained and analyzed by mathematical equations with different levels of biological accuracy. A biological neuron is a dynamical system that produces dynamical behaviors, which can be described by a set of differential equations [13]–[22].

Several biological neuron models have been reported. The most successful and widely used neuron model, the Hodgkin–Huxley (HH) model [23], has been described. The ionic mechanism and electrical current on the membrane surface are taken into consideration in this model. After that, the FitzHugh–Nagumo (FHN) neuron model, which is the simplified version of the HH neuron model, was proposed [24]. The Morris–Lecar neuron model is a conductance-based model, and it was proposed [25] in order to describe oscillations in barnacle giant muscle fiber and is thus biologically significant. The Hindmarsh–Rose (HR) neuron model [26] displays several neuronal behaviors and an accurate output-frequency-to-input-current relationship. In addition to having a simple mathematical description, the Izhikevich neuron model [11] includes very rich neuronal dynamics compared with the HH neuron model.

In all types of neuron models, there are two main mechanisms: First, there are the conductance-based models with high biological precision and high computational cost, such as the HH model, and second, there are the spiking-based models, which describe the temporal behavior of the cortical spikes or spike timing, such as the Izhikevich model. Consequently, there is a tradeoff between model accuracy and its computational complexity.

On the other hand, the main advantage of the HR neuron model is that it is a very simple mathematical neuron model, which describes the thalamic neurons of the brain. A previous software-based work analyzed synchronized networks using HR neuronal models and global couplings [14]–[17], thus motivating the need for an efficient hardware implementation. This desired feature provides the possibility of testing and understanding biological neuron experiments. The implementation of these neuron models on different platforms has been studied such that both analog and digital implementations have been considered. Recently, reconfigurable digital platforms have been used to performed nervous system models [1]–[5], [12], [18]–[20]. Field-programmable gate arrays (FPGAs) are generic programmable digital devices that were used for the implementation of the adaptive-exponential, Izhikevich, FHN, HR, and Morris–Lecar neuron models [1]–[5], [12], [18]–[20]. Although digital computation consumes more silicon area and power per function in comparison with an analog realization, its development time is considerably lower and is robust against power supply fluctuations and thermal noise. The main objective of this brief is to achieve a low hardware overhead and

Manuscript received September 24, 2015; accepted November 21, 2015. Date of publication December 3, 2015; date of current version April 28, 2016. This brief was recommended by Associate Editor T. S. Gotarredona.

M. Hayati is with the Department of Electrical Engineering, Islamic Azad University, Kermanshah 6718997551, Iran, and also with the Faculty of Engineering, Razi University, Kermanshah 6714967346, Iran (e-mail: mohsen_hayati@yahoo.com).

M. Nouri and S. Haghiri are with the Department of Electrical Engineering, Faculty of Engineering, Razi University, Kermanshah 6714967346, Iran (e-mail: moslemnouri70@gmail.com; mo.nouri@pgs.razi.ac.ir).

D. Abbott is with the School of Electrical & Electronic Engineering, The University of Adelaide, Adelaide, SA 5005, Australia (e-mail: derek.abbott@adelaide.edu.au).

Color versions of one or more of the figures in this brief are available online at http://ieeexplore.ieee.org.

Digital Object Identifier 10.1109/TCSII.2015.2505258

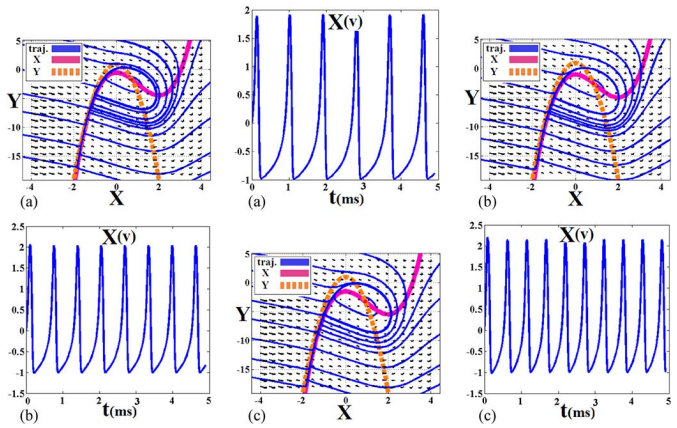

Fig. 1. Spiking mode operation for the HR neuron model at $r = 0.003$. As the stimulus current $I_{\rm app}$ increases, the spiking frequency will be increased. (a) Tonic spiking at $I_{\rm app} = 0.5$ μA. (b) Tonic spiking at $I_{\rm app} = 1$ μA. (c) Tonic spiking at $I_{\rm app} = 1.5$ μA. The orange dashed lines represent Y-nullclinces, pink lines represent X-nullclinces, and blue lines represent the trajectory at black vector fields.

a highly efficient realization of two coupled neurons for use in major neural networks as a main block. This brief presents a significantly simplified implementation of the HR neuron model.

The rest of this brief is organized as follows. Section II presents the dynamics of the HR model, while in Section III, the proposed model is investigated. Section IV presents the dynamical behaviors of synaptic coupling and synchronization. The design and hardware implementation are discussed in Section V. Section VI presents the implementation results. Finally, Section VII concludes this brief.

The equations of the HR model describe the behavior of the neuronal action potential. The HR neuron model can be described by three coupled differential equations as follows:

$$\begin{cases} \frac{dx}{dt} = y - f(x) - z + I_{\rm app} \\ \frac{dy}{dt} = g(x) - y \\ \frac{dz}{dt} = r\left(h(x) - z\right) \end{cases} \tag{1}$$

where

$$\begin{cases} f(x) = x^3 - 3x^2 \\ g(x) = 1 - 5x^2 \\ h(x) = 4\left(x + \frac{8}{5}\right). \end{cases} \tag{2}$$

Here, x is the membrane potential, y is the spiking variable (also known as the recovery current), and z is the bursting variable (also known as the adaptation current). Also, $I_{\rm app}$ is the applied neuron current, and in the presence of spiking behaviors, r controls the spiking frequency, whereas in the case of bursting, r affects the number of spikes per burst.

II. Dynamics of the HR Model

To explain the transition from resting state to spiking state (bifurcation), the interactions of the two nullclines play an important role [19], [27], [28].

As mentioned, the HR neuron model has three coupled equations. On the other hand, based on (1), the z variable of

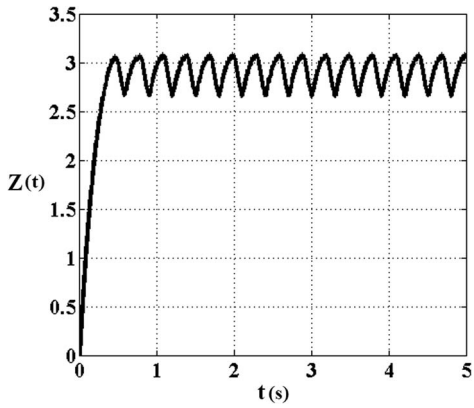

Fig. 2. Simulation result for the bursting variable z. By adjustment of z, the bursting mechanism is enabled.

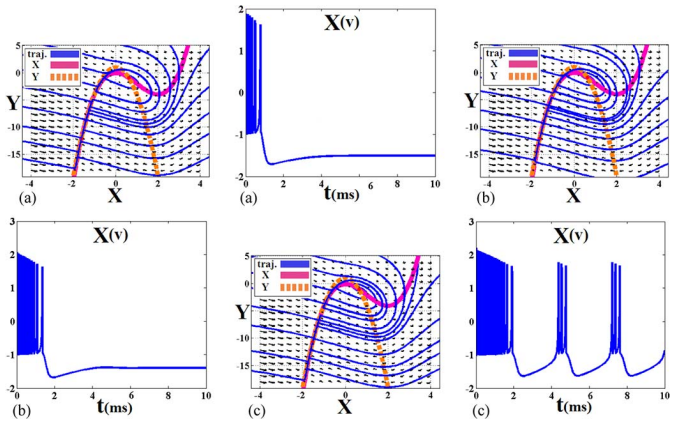

Fig. 3. Bursting mode operation for the HR neuron model at $r = 0.003$. As the stimulus current $I_{\rm app}$ increases, the spiking frequency will be increased. (a) Burst spiking at $I_{\rm app} = 0.5$ μA. (b) Burst spiking at $I_{\rm app} = 1$ μA. (c) Burst spiking at $I_{\rm app} = 1.5$ μA. The orange dashed lines represent Y-nullclinces, pink lines represent X-nullclinces, and blue lines represent the trajectory at black vector fields.

the HR equations is assumed to be a constant value during this analysis, as it is slow when compared to the x and y variables. Thus, this change in the 2-D HR model results in a more accurate frequency–current relationship. In general, two modes of operation can be displayed by the HR neuron model: 1) spiking and 2) bursting.

In the spiking mode, it is assumed that the bursting variable z is equal to zero, and it is a constant value during this analysis. This means that, in spiking mode, the slow z variable remains in a stable equilibrium, and the system is converted to a 2-D model. In this way, the frequency depends on the value of $I_{\rm app}$, and the bursting controller parameter r cannot affect the spiking rate. As depicted in Fig. 1, when $I_{\rm app}$ increases, it becomes an unstable focus with a limit cycle encircling it. As it is shown in this figure, by increasing the stimulus current $I_{\rm app}$, the spiking frequency will be increased. On the other hand, in the bursting mode, the z variable in the HR equations is what provides the bursting patterns. As illustrated in Fig. 2, the z variable has slow variations during time, and by varying this variable in its variation range, we can obtain the bursting operation as demonstrated Fig. 3. The different equilibrium points for two modes have been presented in Table. I.

TABLE I
EQUILIBRIUM POINTS FOR THE SPIKING AND BURSTING MODES

Stimulus current	Nodal Sink (bursting)	Spiral Source (bursting)	Spiral Source (spiking)
0.50 μA	$(-1.61, -12.09)$	$(0.61, -0.90)$	$(0.74, -1.73)$
1.00 μA	$(-1.60, -11.09)$	$(0.60, -1.00)$	$(0.84, -2.52)$
1.50 μA	$(-1.53, -10.70)$	$(0.64, -1.07)$	$(0.92, -3.27)$

TABLE II
HRPWL MODIFIED COEFFICIENTS

coefficient	Approximated Function $p(x)$
$(\mathbf{m_0}, \mathbf{k_0})$	$(-4.00, 1.00)$
$(\mathbf{m_1}, \mathbf{k_1})$	$(-12.00, 7.50)$
$(\mathbf{m_2}, \mathbf{k_2})$	$(-25.50, 29.00)$
$(\mathbf{m_3}, \mathbf{k_3})$	$(-42.00, 86.70)$
$(\mathbf{m_4}, \mathbf{k_4})$	$(-60.00, 176.00)$

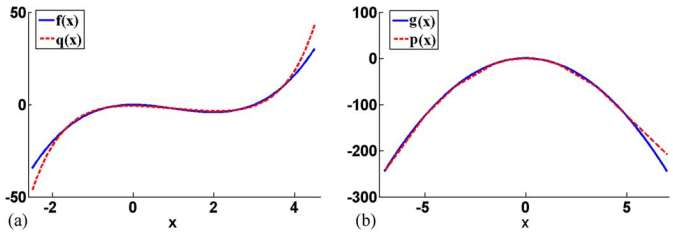

Fig. 4. Matching accuracy. (a) Matching accuracy between f(x) and q(x). (b) Matching accuracy between g(x) and p(x).

III. HR PIECEWISE LINEAR MODEL

In this section, the proposed modification to the original model is presented. The main motivation for these modifications is the implementation cost of the modified design. The membrane potential equation of the HR model can be rewritten as

$$\text{HRPWL}: \begin{cases} \frac{dx}{dt} = y + z - q(x) + I_{\text{app}} \\ \frac{dy}{dt} = p(x) - y \\ \frac{dz}{dt} = r\left(h(x) - z\right) \end{cases} \tag{3}$$

where

$$\begin{cases} (q(x) = (x-1)\left(a2^{(-cx)} + b2^{dx}\right) - 3x + 1 \\ p(x) = \begin{cases} m_0|x| + k_0 & ; \quad X_1 < |x| < X_2 \\ m_1|x| + k_1 & ; \quad X_2 < |x| < X_3 \\ m_2|x| + k_2 & ; \quad X_3 < |x| < X_4 \\ m_3|x| + k_3 & ; \quad X_4 < |x| < X_5 \\ m_4|x| + k_4 & ; \quad \text{else} \end{cases} \\ h(x) = 4\left(x + \frac{8}{5}\right) \end{cases} \tag{4}$$

where $a{=}1.394$, $b{=}0.189$, $c{=}1.40$, $d{=}1.42$, and m_i, $0{<}i{<}4$ are the slopes of lines in the PWL5 approximation of the $p(x)$ function as shown in Table II. Fig. 4 illustrates the matching accuracy between the original HR and HR piecewise linear (HRPWL) neuron models. Fig. 4(b) shows that the $g(x)$ can be approximated by five PWL segments (shown with red dotted lines), representing linear and nonlinear terms in the equation.

The mean absolute error (MAE) is another useful measure widely used in model evaluations. Also, MAE measures how far away predicted values are from observed values and is one of a number of ways to compare forecasts with their eventual outcomes [19]. MAE is a linear score, which means that all the individual differences are weighted equally on the average. As the name suggests, MAE is an average of the absolute errors $|e_i| = |x_{\text{prop}_i} - x_{\text{orig}_i}|$, where x_{prop_i} is the prediction and x_{orig_i} is the true value. In this brief, MAE is given by

$$\text{MAE} = \frac{1}{n}\sum_{i=1}^{n} |e_i|. \tag{5}$$

TABLE III
MAE COMPUTATIONS FOR DIFFERENT STIMULUS CURRENTS WITH TIME STEP = 0.5 MS

r	I_{app} (μA)	MAE
0.005	1.200	0.035
0.001	1.200	0.044
0.002	2.000	0.051
0.008	2.000	0.067
0.030	2.000	0.036
0.030	1.500	0.043
Mean error		**0.046**

According to Table III, the error for each of the input intensities with different frequencies is calculated for a time step of 0.5 ms. Corresponding results indicate an acceptable precision for the proposed method.

IV. SYNAPTIC COUPLING MODEL

In this section, the dynamical behaviors of two coupled HR neurons are presented. Accordingly, we can see the various dynamical behaviors as the current stimulus of the presynaptic neuron, the parameter r that controls the spiking frequency, and the conductance coefficient of the synaptic terminal are varied. The synaptic terminal acts as an active gate, and when the presynaptic voltage level reaches its threshold value, voltage transmission can occur. This state depends on the input stimulus, the coupling of the neurons with the same potentials ($x_{\text{pre}} = x_{\text{post}}$), and when two coupled neurons are synchronized. As mentioned previously, the synchronization effects of coupled neurons are significant for the processing of biological signals and play significant roles in the elucidation of diseases, such as Parkinson's disease, essential tremor, and epilepsy [29]–[31]. Consequently, by the appropriate selection of the input current stimulus and synaptic conductance coefficient, the synchronization effects can be controlled.

This coupled original model is specified as follows:

$$\begin{cases} \frac{dx_{\text{pre}}}{dt} = y_{\text{pre}} - q(x_{\text{pre}}) - z_{\text{pre}} + I_{\text{app}} \\ \frac{dy_{\text{pre}}}{dt} = p(x_{\text{pre}}) - y_{\text{pre}} \\ \frac{dz_{\text{pre}}}{dt} = r\left(h(x_{\text{pre}}) - z_{\text{pre}}\right) \\ \tau_s \frac{dZ}{dt} = \left[1 + \tanh\left(s_s(x_{\text{pre}} - h_s)\right)\right](1 - Z) - \frac{Z}{d_s} \\ I_{\text{syn}} = K_S(Z - Z_0) \\ \frac{dx_{\text{post}}}{dt} = y_{\text{post}} - q(x_{\text{post}}) - z_{\text{post}} + I_{\text{syn}} \\ \frac{dy_{\text{post}}}{dt} = p(x_{\text{post}}) - y_{\text{post}} \\ \frac{dz_{\text{post}}}{dt} = r\left(h(x_{\text{post}}) - z_{\text{post}}\right) \end{cases} \tag{6}$$

where Z is the synaptic activation variable, τ_{s} is the time delay in seconds, S_{s} and d_{s} are responsible for the activation and relaxation of Z, h_{s} is the threshold parameter for the activation

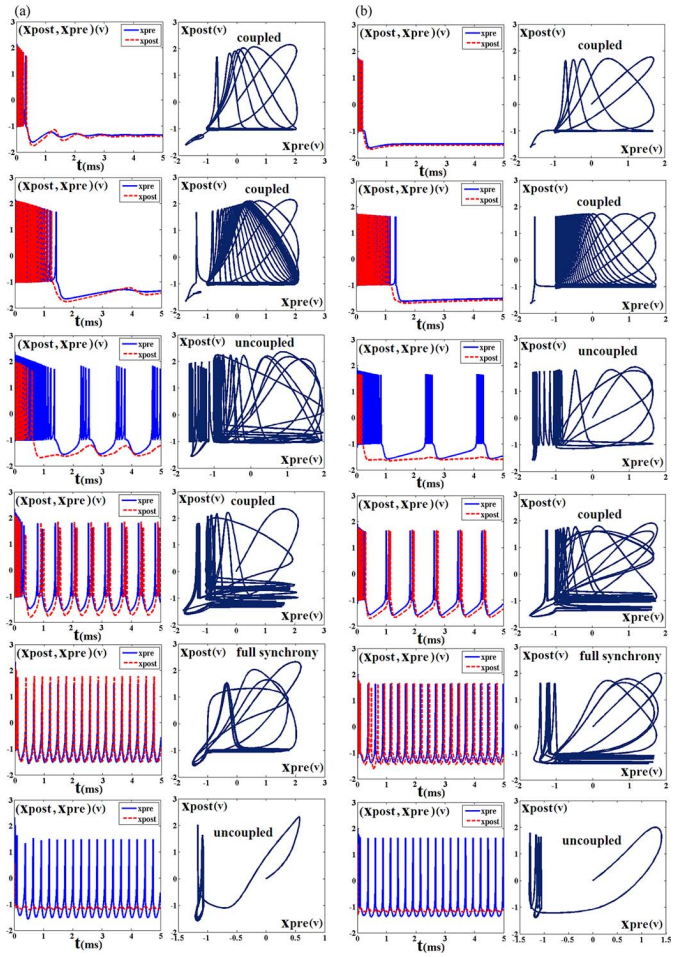

Fig. 5. Dynamic behavior and phase portraits of two coupled HR neurons with different values of current stimulus, conductance coefficient, and spiking parameter r. For $I_{\text{stimulus}} = 2$, $K_S = 3$, and $r = 0.03$, full synchrony will occur. (a) Synaptic coupling of the original HR model. (b) Synaptic coupling of the proposed HR model. The spans of the current stimulus, conductance coefficient, and spiking parameter are 0.5 to 3 μA with increase step $= 0.5$ μA, 0 to 5 with increase step $= 1$, and 0 to 0.05 with increase step $= 0.01$, respectively.

of Z, I_{syn} is the synaptic current, k_{s} plays the role of conductance, and Z_0 is the reference level of Z. Fig. 5 shows the different behaviors of two coupled neurons. In the general case, for specific values of the stimulus current (I_{stimulus}), r, and K_S, the synchronization effect can be observed. As demonstrated in Fig. 5, the proposed model can mimic the biological HR model with high precision.

V. Design and Hardware Implementation

This section presents the hardware implementation structure for the proposed model. In order to obtain an improved comparison in the number of used multipliers between the original and proposed models, according to (1)–(4), the scheduling diagrams (data flow graph with scheduling control steps) of the original and proposed models are drawn in Fig. 6.

As the first step, it is necessary to discretize equations for both models; therefore, we utilize the Euler method. The second step is the bit-width determination of the hardware functional units. The span of the membrane potential is -2 to 2 V, and

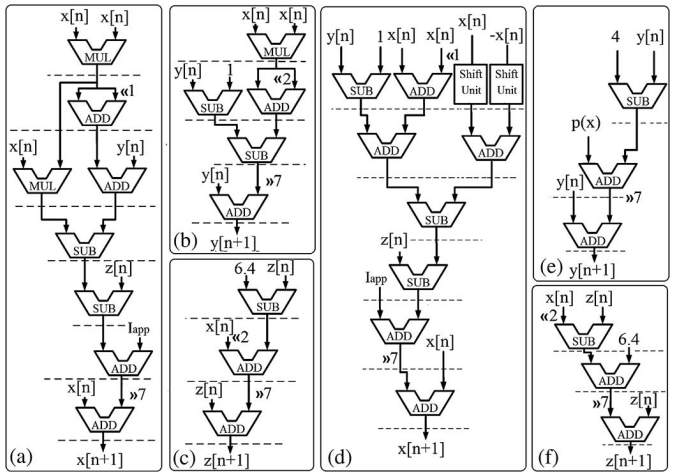

Fig. 6. Scheduling diagram of the original and proposed models. (a) Membrane potential x of the original model. (b) Recovery variable y of the original model. (c) Bursting variable z of the original model. (d) Membrane potential x of the proposed model. (e) Recovery variable y of the proposed model. (f) Bursting variable z of the proposed model.

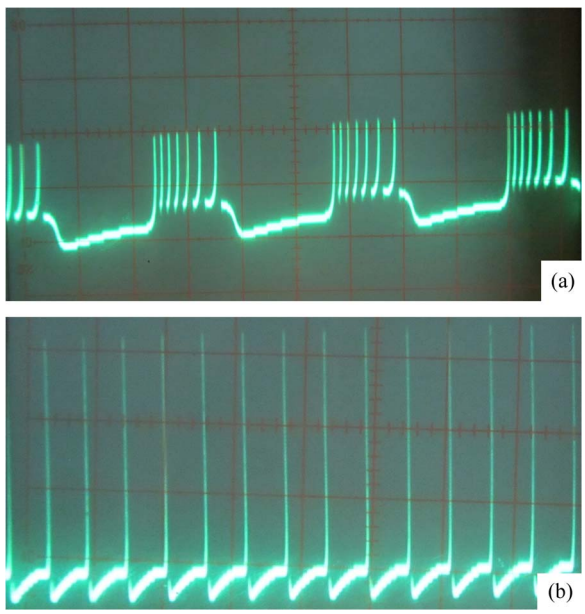

Fig. 7. Oscilloscope photographs, which show the effect of varying parameters in terms of different spiking patterns. (a) Tonic bursting. (b) Tonic spiking. The horizontal axis denotes time (time scale $= 10$ ms), and the vertical axis shows voltage (voltage scale $= 25$ mV).

the minimum bits for implementing the membrane potentials are 3 b. In the bit-width determination, if the maximum logic shifts to the right or left are not considered, then overflow can occur. To avoid any overflow and also increasing accuracy of the calculations, a bit width of 20 that consists of 8 b for the integer part and 12 b for the fraction is considered.

VI. Implementation Results

Circuits are implemented on a XILINX Virtex-II Pro development system. Fig. 7 shows the oscilloscope photographs of the dynamical behavior of a single neuron implemented on this FPGA platform using HR and the proposed models. The device utilization for the implementation of the proposed models is

TABLE IV
DEVICE UTILIZATION OF THE XILINX VIRTEX-II PRO. ABBREVIATIONS: RESOURCE (RES.), UTILIZATION (UTIL.), AVAILABLE (AV.), FF' SLICE (FF' S.), 4 INPUT LUTS (LUTS), BONDED IOBS (IOBS), MULT18 × 18 S (MU.), AND FREQUENCY (FREQ.)

	Original model		Proposed model		
Res.	Used	Util.	Used	Util.	Av.
Slices	288	2%	412	3%	13696
FF' S	301	1%	431	1%	27392
LUTs	442	1%	659	2%	27392
IOBs	64	11%	64	11%	556
MU	12	8%	0	0%	136
GCLKs	1	6%	1	6%	16
Freq.	23.7 MHz		81.2 MHz		400 MHz

summarized in Table IV. The results of hardware implementation show that the proposed model is low cost compared to the implementation of the original HR neuron model, and this is expected because hyperbolic terms and multiplications require a high area consumption for a circuit implementation. In the proposed model implementation, multipliers are eliminated but with an increase in the number of slices. However, calculations show that there is approximately a 0.77% overall saving in the FPGA area for a given frequency. However, there is a tradeoff, and for a given area, the new implementation offers about a 14.37% speedup.

VII. CONCLUSION

A multiplierless piecewise linear model based on the HR model, targeting a low-cost digital implementation, has been presented. Simulation results and hardware realization show that the proposed model has acceptable error and is suitable for digital implementation. This proposed model has lower computational and hardware costs compared with the original HR neuron model. This system is conveniently implemented on FPGA. This hardware is used to demonstrate different dynamics of the HR neuron model, depending on the parameter values and current stimulus, producing different patterns of spiking activity with minimal computational error.

REFERENCES

[1] A. Kazemi, A. Ahmadi, and S. Gomar, "A digital synthesis of Hindmarsh-Rose neuron: A thalamic neuron model of the brain," in *Proc. 22nd ICEE*, 2014, pp. 238–241.

[2] S. Haghiri, A. Ahmadi, M. Nouri, and M. Hiedarpur, "An investigation on neuroglial interaction effect on Izhikevich neuron behaviour," in *Proc. 22nd ICEE*, 2014, pp. 88–92.

[3] M. Nouri, Gh. R. Karimi, A. Ahmadi, and D. Abbott, "Digital multiplierless implementation of the biological FitzHugh-Nagumo model," *Neurocomputing*, vol. 165, pp. 468–476, Oct. 2015.

[4] M. Hayati, M. Nouri, S. Haghiri, and D. Abbott, "A digital realization of astrocyte and neural glial interactions," *IEEE Trans. Biomed. Circuits Syst.*, vol. 10, no. 1, pp. 518–529, Apr. 2016.

[5] T. Hishiki and H. Torikai, "A novel rotate-and-fire digital spiking neuron and its neuron-like bifurcations and responses," *IEEE Trans. Neural Netw.*, vol. 22, no. 5, pp. 752–767, May 2011.

[6] L. Geretti and A. Abramo, "The correspondence between deterministic and stochastic digital neurons: Analysis and methodology," *IEEE Trans. Neural Netw.*, vol. 19, no. 10, pp. 1739–1752, Oct. 2008.

[7] R. Serrano-Gotarredona *et al.*, "CAVIAR: A 45 k neuron, 5M synapse, 12G connects/s AER hardware sensory-processing-learning-actuating system for high-speed visual object recognition and tracking," *IEEE Trans. Neural Netw.*, vol. 20, no. 9, pp. 1417–1438, Sep. 2009.

[8] R. J. Vogelstein, U. Mallik, J. T. Vogelstein, and G. Cauwen-berghs, "Dynamically reconfigurable silicon array of spiking neurons with conductance-based synapses," *IEEE Trans. Neural Netw.*, vol. 18, no. 1, pp. 253–265, Jan. 2007.

[9] R. Serrano-Gotarredona, T. Serrano-Gotarredona, A. Acosta-Jimenez, and B. Linares-Barranco, "A neuromorphic cortical-layer microchip for spike-based event processing vision systems," *IEEE Trans. Circuits Syst. I, Reg. Papers*, vol. 53, no. 12, pp. 2548–2566, Dec. 2006.

[10] S. B. Furber, S. Temple, and A. D. Brown, "High-performance computing for systems of spiking neurons," in *Proc. AISB Workshop GC5, Archit. Brain Mind*, 2006, vol. 2, pp. 29–36.

[11] E. M. Izhikevich, "Simple model of spiking neurons," *IEEE Trans. Neural Netw.*, vol. 14, no. 6, pp. 1569–1572, Nov. 2003.

[12] S. Gomar and A. Ahmadi, "Digital multiplierless implementation of biological adaptive-exponential neuron model," *IEEE Trans. Circuits Syst. I, Reg. Papers*, vol. 61, no. 4, pp. 1206–1219, Apr. 2013.

[13] T. Yu and G. Cauwenberghs, "Analog VLSI biophysical neurons and synapses with programmable membrane channel kinetics," *IEEE Trans. Biomed. Circuits Syst.*, vol. 4, no. 3, pp. 139–148, Jun. 2010.

[14] S. D. Djeundam, R. Yamapi, G. Filatrella, and T. C. Kofane, "Stability of the synchronized network of Hindmarsh–Rose neuronal models with nearest and global couplings," *Commun. Nonlinear Sci. Numer. Simul.*, vol. 22, no. 1–3, pp. 545–563, May 2015.

[15] H. Yu and J. Peng, "Chaotic synchronization and control in nonlinear-coupled Hindmarsh–Rose neural systems," *Chaos Solitons Fractals*, vol. 29, no. 2, pp. 342–348, Jul. 2006.

[16] D.-Q. Wei and X.-S. Luo, "Coherence resonance and noise-induced synchronization in Hindmarsh–Rose neural network with different topologies," *Commun. Theor. Phys.*, vol. 48, no. 4, pp. 759–762, Oct. 2007.

[17] C. Murguia, R. H. Fey, and H. Nijmeijer, "Network synchronization of time-delayed coupled nonlinear systems using predictor-based diffusive dynamic couplings," *Chaos, Interdisc. J. Nonlinear Sci.*, vol. 25, no. 2, Feb. 2015, Art. no. 023108.

[18] M. Hayati, M. Nouri, S. Haghiri, and D. Abbott, "Digital multiplierless realization of two coupled biological Morris-Lecar neuron model," *IEEE Trans. Circuits Syst. I, Reg. Papers*, vol. 62, no. 7, pp. 1805–1814, Jul. 2015.

[19] M. Nouri *et al.*, "A Hopf resonator for 2-D artificial cochlea: Piecewise linear model and digital implementation," *IEEE Trans. Circuits Syst. I, Reg. Papers*, vol. 62, no. 4, pp. 1117–1125, Apr. 2015.

[20] H. Soleimani, M. Bavandpour, A. Ahmadi, and D. Abbott, "Digital implementation of a biological astrocyte model and its application," *IEEE Trans. Neural Netw. Learn Syst.*, vol. 26, no. 1, pp. 127–139, Mar. 2014.

[21] J. Misra and I. Saha, "Artificial neural networks in hardware: A survey of two decades of progress," *Neurocomputing*, vol. 74, no. 1–3, pp. 239–255, Dec. 2010.

[22] E. Farquhar and P. Hasler, "A bio-physically inspired silicon neuron," *IEEE Trans. Circuits Syst. I, Reg. Papers*, vol. 52, no. 3, pp. 477–488, Mar. 2005.

[23] A. L. Hodgkin and A. F. Huxley, "A quantitative description of membrane current and its application to conduction and excitation in nerve," *J. Physiol.*, vol. 117, no. 4, pp. 500–544, Aug. 1952.

[24] R. FitzHugh, "Impulses and physiological states in theoretical models of nerve membrane," *J. Biophys.*, vol. 1, no. 6, pp. 445–466, Jul. 1961.

[25] C. Morris and H. Lecar, "Voltage oscillations in the barnacle giant muscle fiber," *J. Biophys.*, vol. 35, no. 1, pp. 193–213, Jul. 1981.

[26] R. M. Rose and J. L. Hindmarsh, "The assembly of ionic currents in a thalamic neuron. I. The three-dimensional," *Proc. R. Soc. Lond. B, Biol. Sci.*, vol. 237, no. 1288, pp. 267–288, Aug. 1988.

[27] M. R. Azghadi, S. F. Al-Sarawi, D. Abbott, and N. Iannella, "A neuromorphic VLSI design for spike timing and rate based synaptic plasticity," *Neural Netw.*, vol. 45, pp. 70–82, Sep. 2013.

[28] M. F. Simoni and S. P. DeWeerth, "Adaptation in a VLSI model of a neuron," *IEEE Trans. Circuits Syst. II, Analog Digit. Signal Process.*, vol. 46, no. 7, pp. 967–970, Jul. 2002.

[29] W. W. Albert, E. J. Wright, and B. Feinstein, "Cortical potentials and Parkinsonian tremor," *Nature*, vol. 221, no. 5181, pp. 670–672, Feb. 1969.

[30] C. A. S. Batista, S. R. Lopes, R. L. Viana, and A. M. Batista, "Delayed feedback control of bursting synchronization in a scale-free neuronal network," *Neural Netw.*, vol. 23, no. 1, pp. 114–124, Jan. 2010.

[31] H. Yu, J. Wang, Q. Liu, B. Deng, and X. Wei, "Delayed feedback control of bursting synchronization in small-world neuronal networks," *Neurocomputing*, vol. 99, pp. 178–187, Jan. 2013.